Article

Not peer-reviewed version

Amphiphilic Diblock Copolymers of Poly (N-Vinyl Pyrrolidone) and Poly (Vinyl Esters) Bearing N-Alkyl Side Chains for the Encapsulation of Curcumin and Indomethacin

Nikolaos V. Plachouras , Aikaterini Maria Gkolemi , Alexandros Argyropoulos , Athanasios Bouzoukas , Theodosia Panagiota Papazoglou , Nikoletta Roka , Marinos Pitsikalis *

Posted Date: 30 September 2025

doi: 10.20944/preprints202509.2475.v1

Keywords: amphiphilic block copolymers; poly(N-vinyl pyrrolidone); poly(n-alkyl vinyl esters); self-assembly; polymeric micelles; drug encapsulation; curcumin; indomethacin; light scattering

Article

Amphiphilic Diblock Copolymers of Poly (N-Vinyl Pyrrolidone) and Poly (Vinyl Esters) Bearing N-Alkyl Side Chains for the Encapsulation of Curcumin and Indomethacin

Nikolaos V. Plachouras, Aikaterini-Maria Gkolemi, Alexandros Argyropoulos, Athanasios Bouzoukas, Theodosia-Panagiota Papazoglou, Nikoletta Roka and Marinos Pitsikalis *

Industrial Chemistry Laboratory, Department of Chemistry, National and Kapodistrian University of Athens, Panepistimiopolis Zografou, 15771 Athens, Greece
* Correspondence: pitsikalis@chem.uoa.gr; Tel.: +30-210-727-4768

Abstract

This study investigates the self-assembly behavior of a series of amphiphilic diblock copolymers, each consisting of a hydrophilic poly(N-vinyl pyrrolidone) (PNVP) block and a hydrophobic block derived from n-alkyl vinyl esters, namely poly(vinyl butyrate) (PVBu), poly(vinyl decanoate), (PVDc) and poly(vinyl stearate) (PVSt), in aqueous solutions. Dynamic and static light scattering (DLS and SLS) techniques were employed to monitor the micellization behavior. The effect of the nature of the hydrophobic block, the copolymer composition and the copolymer molecular weight on the self-assembly properties were thoroughly examined. The encapsulation of curcumin and indomethacin within the dry cores of the micellar structures was conducted in aqueous solutions for all block copolymers at various curcumin/indomethacin-to-polymer mass ratios. UV-Vis spectroscopy was used to evaluate the drug loading capacity and efficiency (%DLC and %DLE). In several cases, the encapsulation of both hydrophobic drugs was found to be nearly quantitative. Combined with the observed stability of the micellar structures, these findings suggest that the block copolymers demonstrate significant potential as carriers for drug delivery applications.

Keywords: amphiphilic block copolymers; poly (N-vinyl pyrrolidone); poly (n-alkyl vinyl esters); self-assembly; polymeric micelles; drug encapsulation; curcumin; indomethacin; light scattering

1. Introduction

A major obstacle in the efficient development of pharmaceuticals is still their limited solubility in aqueous media. Despite efforts to address this issue, over 40% of licensed medications and up to 90% of investigational substances exhibit low solubility in water, according to estimates. [1] The proliferation of barely water-soluble drug candidates, which is attributed to the strategic application of combinatorial chemistry and the routine implementation of high-throughput screening in non-aqueous systems [2,3], is typically accompanied by a range of associated problems. Their poor water solubility lowers their pharmacological potential by restricting dissolution and absorption, promoting aggregation or premature precipitation in aqueous environments that may result in recrystallization and variable pharmacokinetics, and facilitating rapid systemic clearance through tissue distribution, plasma protein binding, or accelerated elimination. Furthermore, their clinical activity is further limited by intrinsic chemical and oxidative instability before they reach the target site. [4–7]

An effective strategy to overcome the aforementioned limitations is the employment of biocompatible amphiphilic block copolymers, capitalizing on their spontaneous self-assembling into

 doi:10.20944/preprints202509.2475.v1

micelles in aqueous solutions. The hydrophobic core of the micelles can encapsulate therapeutic molecules that would otherwise be insoluble in water, enhancing their apparent solubility and preventing the degradation of the active ingredient. [8,9] Moreover, the hydrophilic shell of the micelles confers colloidal stability, extending their circulation half-life and biodistribution. The tunable architecture of block copolymers enables high drug loading and controlled release profiles. This can be achieved by adding functional groups to target specific tissues or tumors, or by including pH- or redox-responsive functionalities. [10–12] Finally, the broad spectrum of available loading methods, including thin-film hydration, solvent evaporation, dialysis and co-solvent methods facilitates optimization of micellar formulation for a wide variety of hydrophobic drugs. [13]

Curcumin is a highly hydrophobic molecule with extremely low water solubility, which limits its bioavailability. It is considered a natural ingredient that has sparked scientific interest due to its numerous advantages on human health, as it is believed to have anti-inflammatory, antioxidant, antibacterial, antiviral, antifungal, antidiabetic, and anticancer properties. [14] Another practically water-insoluble molecule with particularly interesting pharmacological properties is indomethacin. It belongs to the class of nonsteroidal anti-inflammatory drugs (NSAIDs) and has been clinically employed for the treatment of acute pain, rheumatoid arthritis, ankylosing spondylitis, osteoarthritis, bursitis, gouty arthritis, patent ductus arteriosus, and certain types of migraine. [15] Both curcumin and indomethacin can easily be traced by UV-Vis spectroscopy since they exhibit a maximum absorption at 429 nm [16] and 318 nm [17], respectively. The chemical structures of both curcumin and indomethacin are shown in Scheme 1.

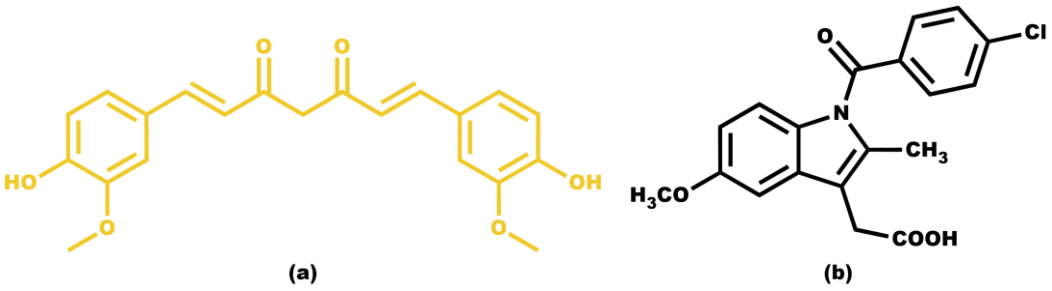

Scheme 1. (a) Chemical structure of the hydrophobic drug compound curcumin; (b) Chemical structure of the hydrophobic drug compound indomethacin.

This study investigates the micellization behavior of a series of amphiphilic diblock copolymers, each consisting of a hydrophilic poly(N-vinyl pyrrolidone) (PNVP) block and a hydrophobic block derived from n-alkyl vinyl esters, namely poly(vinyl butyrate) (PVBu), poly(vinyl decanoate), (PVDc) and poly(vinyl stearate) (PVSt), in aqueous solutions. The chemical structures of each different family of amphiphilic diblock copolymers are demonstrated in Scheme 2. Poly(N-vinyl pyrrolidone) possesses distinctive properties, including biocompatibility and non-toxicity, which has led to its extensive industrial utilization in the pharmaceutical and biomedical, among other sectors. [18] In fact, recent studies suggest PNVP as the optimal choice for replacing poly(ethylene oxide) (PEO), which is currently the most widely used hydrophilic material employed in the aforementioned sectors. [19,20] Poly(vinyl esters) (PVEs) represent another significant class of polymeric materials, which exhibit either hydrophilic or hydrophobic characteristics, depending on the nature of the side group. These materials are of pharmacological significance due to their capability to serve as precursors for the production of poly(vinyl alcohol) (PVA) through the process of hydrolysis of their ester group. [21,22]

 doi:10.20944/preprints202509.2475.v1

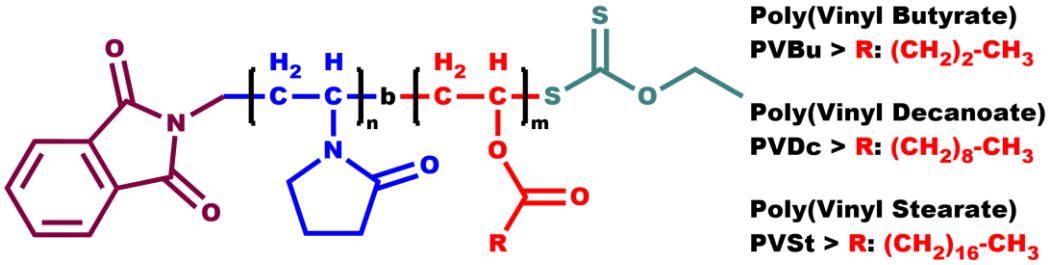

Scheme 2. Chemical structures of the amphiphilic diblock copolymers consisting of a hydrophilic PNVP block and a hydrophobic block derived from PVBu, PVDc and PVSt.

The micellization behavior of amphiphilic block copolymers is governed by a delicate balance of molecular and environmental parameters. The length of the hydrophobic chain and the molecular weight of the copolymers are two of the primary determinants. Longer alkyl chains markedly reduce the critical micelle concentration (CMC) and promote the formation of larger, more stable aggregates, as the increased hydrophobic interactions drive self-assembly. [23,24] Similarly, higher molecular weights of amphiphilic block copolymers favor micellization by lowering the CMC and enabling the formation of well-defined, stable micelles with improved thermodynamic stability. [25,26] The present study aims to assess the aforementioned factors by examining the self-assembly behavior in water, of a series of the previously mentioned amphiphilic diblock copolymers. Parameters, such us the nature of the different PVEs blocks, the molecular weight and the composition where examined to affect the micellization behavior.

Water was selected as the solvent in the micellization study, as it is a selective solvent for the water-soluble PNVP blocks. [27–29] The self-assembly behavior of the same series of diblock copolymers in tetrahydrofuran (THF) has been already presented. [30] In addition to micellization study, the two hydrophobic drugs, curcumin and indomethacin were successfully encapsulated into the core of the micellar structures formed, with the calculated drug loading capacity and efficiency (%DLC and %DLE) values [31] indicating that these amphiphilic block copolymers have significant potential as carriers for drug delivery applications.

2. Materials and Methods

2.1. Synthesis of Diblock Copolymers PNVP-b-PVBu, PNVP-b-PVDc and PNVP-b-PVSt

The synthesis of the PNVP based amphiphilic diblock copolymers has already been published. [32] In summary, the synthesis of the copolymers was accomplished through the implementation of the reversible addition-fragmentation chain transfer (RAFT) radical polymerization technique, in conjunction with the sequential addition of monomers. In each instance, the PNVP block was synthesized first and after purification and characterization was used as a macro chain transfer agent (macro-CTA) for the polymerization of each PVE block. For each of the three distinct copolymer classes, designated PNVP-b-PVBu, PNVP-b-PVDc, and PNVP-b-PVSt, a total of four or five different copolymers with varying molecular weights and molar ratio of each block were synthesized in order to investigate the effect of these parameters on the micellization behavior of the products in aqueous solutions. In order to correlate these parameters with the results and for convenience, it is necessary to list them, and they are therefore summarized in Table 1.

Table 1. Molecular characteristics of the PNVP-b-PVEs amphiphilic diblock copolymers.

Sample	PNVP [1]		PNVP-b-PVEs [1]		NVP [2]	PVEs [2]
	M_n x10³ (Da)	Đ	M_n x10³ (Da)	Đ	molar ratio (%)	molar ratio (%)
PNVP-b-PVBu #1	8.5	1.30	16.0	1.90	22	78
PNVP-b-PVBu #2	28.0	1.27	32.0	1.32	84	16
PNVP-b-PVBu #3	8.9	1.35	17.5	1.40	57	43

 doi:10.20944/preprints202509.2475.v1

PNVP-b-PVBu #4	8.9	1.35	15.5	1.54	48	52
PNVP-b-PVBu #5	8.5	1.30	13.0	1.55	56	44
PNVP-b-PVDc #1	8.5	1.30	12.5	1.31	63	37
PNVP-b-PVDc #2	5.5	1.47	12.5	1.60	38	62
PNVP-b-PVDc #3	8.5	1.30	11.0	1.45	56	44
PNVP-b-PVDc #4	9.5	1.36	10.5	1.36	93	7
PNVP-b-PVSt #1	8.5	1.30	10.5	1.44	78	22
PNVP-b-PVSt #2	7.5	1.30	10.4	1.51	61	39
PNVP-b-PVSt #3	8.1	1.30	10.9	1.37	85	15
PNVP-b-PVSt #4	8.1	1.30	12.5	1.22	83	17
PNVP-b-PVSt #5	5.5	1.47	9.0	1.62	40	60

[1] Derived by seize exclusion chromatography (SEC) in $CHCl_3$. [2] Derived by ^{1}H-NMR in $CDCl_3$.

2.2. Dynamic and Static Light Scattering (DLS and SLS) Techniques

2.2.1. Preparation of Stock Solutions for the DLS and SLS Measurements

The solvent exchange method was selected for the preparation of stock solutions for each of the distinct samples in each of the three different types of diblock copolymers. Specifically, 20 mg of each sample were initially dissolved in 5 mL of dry THF in a vial. The THF had been dried overnight over sodium and distilled prior to use. The samples were left in THF overnight to ensure complete dissolution of the diblock copolymers. Thereafter, 20 mL of extra pure water was added to each vial. Subsequently, the solutions were heated at 65 °C to guarantee full evaporation of the THF, thereby enabling the self-assembly of the amphiphilic diblock copolymers in water. The initial concentrated solution of each sample, with a concentration of about 10^{-3} g/mL, was further diluted to different lower concentrations. For the SLS measurements, the stock solutions of each sample were prepared via the exact same procedure.

2.2.2. Instrumentation and Methods for the DLS and SLS Measurements

Both DLS and SLS measurements were performed on a NanoBrook Omni system from Brookhaven Instruments. The instrument was equipped with a Cyonics Ar^+ laser operating at 640 nm with variable power, a PCS8 temperature regulator, an RR98 pump and filtering module, and a 510-channel correlator used for data collection. For the DLS experiments, correlation functions were collected at 25 °C at a 90° scattering angle and analyzed by the cumulant method and the CONTIN software. [33] Measurements were carried out ten times for each concentration of each sample and were averaged. Before each measurement, all solutions were filtered using a 25 mm PVDF hydrophilic welded syringe filter with 0.45 μm pore size and directly introduced into the scattering cell. SLS experiments were conducted at the same temperature and scattering angle.

The intensity time autocorrelation function, $g_2(q,t)$, was determined following standard procedures, where q is the scattering vector, t the time, and t_0 the lag time. The scattering vector was defined as $q = \frac{4\pi n_0}{\lambda}\sin\left(\frac{\theta}{2}\right)$, with θ being the observation angle, n_0 the refractive index of the solvent, and λ the wavelength of the incident light.

As mentioned, the autocorrelation functions were analyzed using the cumulant method. The normalized electric field autocorrelation function can be expressed as: $g_1(t) = \int_0^\infty G(\Gamma)e^{-\Gamma t}d\Gamma$ where $G(\Gamma)$ is the distribution of decay rates and Γ the average decay rate. In the cumulant expansion, this is written as: $g_1(t) = \exp\left(-\Gamma t + \frac{\mu_2}{2!}t^2 - \frac{\mu_3}{3!}t^3 + \cdots\right)$ where Γ is the average decay rate of the correlation function, and μ_2 is the second cumulant describing the variance of the distribution. The polydispersity index (PDI) was calculated as: $PDI = \frac{\mu_2}{\Gamma^2}$ providing a quantitative measure of the distribution width of the relaxation times. From the mean decay rate, the apparent translational diffusion coefficients were obtained. Extrapolation to zero concentration yielded $D_{0,app}$ while the apparent hydrodynamic radii, R_h^0, were obtained from the Stokes–Einstein relation: $R_h^0 = \frac{kT}{6\pi\eta_S D_{0,app}}$ where k is the Boltzmann constant, T the absolute temperature, and η_s the solvent viscosity. The

 doi:10.20944/preprints202509.2475.v1

concentration dependence of the diffusion coefficient was described by $D = D_{0,app}(1 + k_D c)$, where k_D denotes the diffusion interaction parameter.

Furthermore, k_D is related to the second virial coefficient A_2 according to: $k_D = 2A_2M + k_f - u$ where M is the molecular weight, k_f the concentration dependence of the friction coefficient, and u the polymer's partial specific volume.

SLS data were processed according to the Debye formalism, employing the equation: $\frac{Kc}{\Delta R_\theta} = \frac{1}{M_w} + 2A_2c$ where the optical constant K is an optical constant incorporating the refractive index increment dn/dc, and ΔR_θ represents the excess Rayleigh ratio relative to the solvent. Refractive index increments measurements were performed on a Chromatix KMX-16 refractometer from Milton Roy, operating at 633 nm and calibrated with aqueous NaCl solutions. These analyses enabled the determination of molecular weight and second virial coefficient values.

2.3. Encapsulation of Curcumin and Indomethacin

2.3.1. Preparation of Stock Solutions for Drug Encapsulation

The stock solutions employed for the study of the encapsulation of curcumin and indomethacin within the dry core of the micellar structures formed by the amphiphilic diblock copolymers in water, were prepared with the same methodology as those utilized for the DLS and SLS measurements. The sole discrepancy is as follows. The initial solution of the diblock copolymer, dissolved in THF, was equally distributed between separate vials. Before the addition of only 5 mL of extra pure water in this occasion, a solution of the drug in THF was introduced to these vials at varying drug-to-polymer mass ratios. The vials were then left overnight to ensure full interaction between the drug and the polymer. Subsequently, the remaining steps of the procedure were identical to those previously mentioned.

At this point, it would be beneficial to provide a concrete illustration concerning concentrations. Approximately 20 mg of a sample are dissolved in 20 mL of dry THF. This solution is equally divided into 5mL proportions in four vials. To these vials, a solution of indomethacin in THF is introduced at concentrations of 10, 15 and 20 % w/w indomethacin or curcumin/polymer. The solution that remains without the administration of a drug is utilized as a blank for the UV-Vis measurements, as described in the forthcoming section. The precise concentrations of polymers and drugs are provided, along with the results obtained in the Results and Discussion section.

2.3.2. Drug Loading Capacity and Efficiency (%DLC and %DLE) Calculation

It has previously been established that both curcumin and indomethacin absorb at 429 and 320 nm, respectively. Consequently, UV-Vis spectroscopy was employed for their quantitative determination in the solutions in which their encapsulation was attempted. The experiments were conducted on a Lamda 650 spectrophotometer from Perkin Elmer, operating within a wavelength range of 250 to 800 nm, at 25 °C, using a 3 mL quartz cell.

Initially, two separated calibration curves were created from UV-Vis spectroscopy, measuring the absorbance of curcumin and indomethacin solutions in THF with varying concentrations. Using the corresponding calibration curve and measuring the absorbance of the polymer solutions with the encapsulated drugs, two critical parameters, namely drug loading capacity (%DLC) and drug loading efficiency (%DLE), were evaluated via the following equations:

$$Drug\ Loading\ Capacity\ (DLC)\ \% = \frac{mass\ of\ loaded\ drug}{mass\ of\ polymer} * 100 \quad (1)$$

$$Drug\ Loading\ Efficiency\ (DLE)\ \% = \frac{mass\ of\ loaded\ drug}{mass\ of\ drug\ in\ feed} * 100 \quad (2)$$

3. Results and Discussion

3.1. Self-Assembly Behavior of the Amphiphilic Diblock Copolymers in Aqueous Solutions

 doi:10.20944/preprints202509.2475.v1

3.1.1. DLS Results for the PNVP-b-PVBu Samples

As illustrated in Table 1, sample PNVP-b-PVBu #2 exhibits the highest percentage of the PNVP block and the lowest percentage of the PVBu block among the other PNVP-b-PVBu samples. This suggest that the micellar structures formed from this sample in water are expected to have a large sized shell and a small sized core, thus falling under the classification of the star-like micelles. In contrast, sample PNVP-b-PVBu #1 represents the opposite extreme, containing the highest percentage of the PVBu block and the lowest percentage of the PNVP block . Consequently, the expected morphology of the micellar structures formed from this sample is reversed, featuring a comparatively thin shell and an expanded core, which places it in the category of crew-cut micelles. The remaining three samples have a roughly equivalent PNVP block yet varying from each other in terms of the percentage of their hydrophobic PVBu block.

The experimental results of the DLS analysis for the PNVP-b-PVBu samples are summarized in Table 2 and representative DLS plots are displayed in Figure 1.

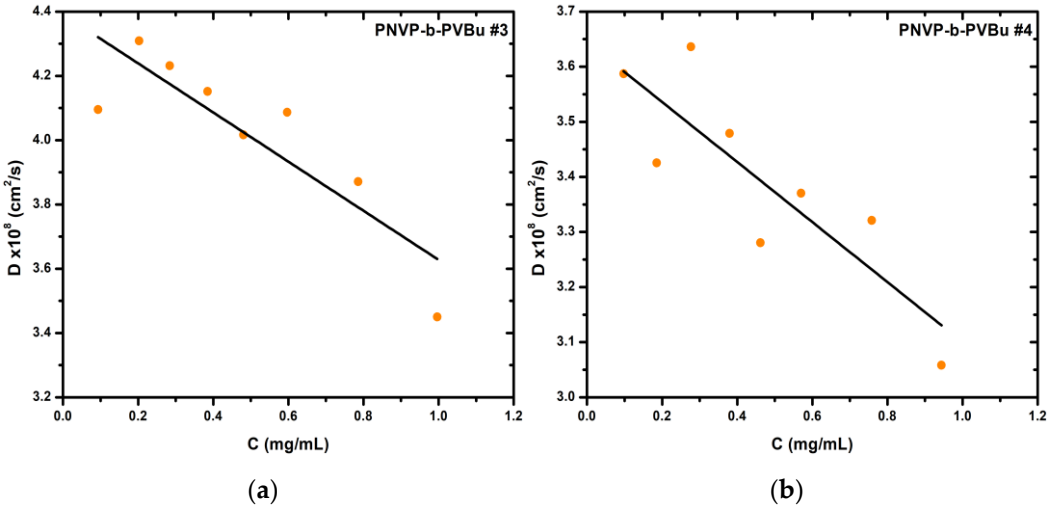

(**a**) (**b**)

Figure 1. (a) DLS plot of sample PNVP-b-PVBu #3; (b) DLS plot of sample PNVP-b-PVBu #4.

Table 2. DLS results for the PNVP-b-PVBu samples.

Sample	D_0 x10⁸ (cm/s²)	K_D	R_{h0} (nm)	$R_{h1,0}$ (nm)	$R_{h2,0}$ (nm)
PNVP-b-PVBu #1	2.653	-86.11	92.4	-	-
PNVP-b-PVBu #2	4.813	177.46	50.9	30.8	127.6
PNVP-b-PVBu #3	4.392	-174.02	55.8	23.1	104.6
PNVP-b-PVBu #4	3.645	-149.42	67.3	29.5	99.2
PNVP-b-PVBu #5	6.198	362.45	39.6	20.3	115.7

Sample PNVP-b-PVBu #1, which contains the highest percentage of the PVBu block, according to CONTIN analysis and the results demonstrated in Table 2, exhibits only a single population of particles in aqueous solutions with $R_{h0} = 92.4$ nm, and a polydispersity index of $0.1 < PDI < 0.2$. This finding suggest that the supramolecular structures formed are relatively uniform, most notably when considering the relatively broad polydispersity, $Đ = 1.90$, of the initial diblock copolymer PNVP-b-PVBu #1. This result, in conjunction with the large size of detected structures, indicates the presence of either micellar aggregates or vesicles.

In contrast with the sample PNVP-b-PVBu #1, the remaining samples with the lower percentage of the hydrophobic PVBu block, as revealed by CONTIN analysis and the results presented in Table 2, exhibit two distinct populations with dimensions ranging from 20 to 30 nm and 100 to 130 nm, respectively. Taking into consideration the low molecular weights of the diblock copolymers, it can be concluded that there is an equilibrium between micelles and either micellar aggregates or vesicles.

 doi:10.20944/preprints202509.2475.v1

In each sample, the overall PDI attains relatively high values, due to the aforementioned equilibrium, however, each individual population exhibits a notable uniform size, a finding that is in alignment with the observations derived from sample PNVP-b-PVBu #1.

In the case of the sample PNVP-b-PVBu #2, a substantial enhancement in the fraction of micellar aggregates or vesicles was observed, with an increase from 30% at low concentrations up to 55% at high concentrations, upon increasing concentration the micellar structures approach one-another closer, thereby facilitating interactions mediated by the hydrophilic PNVP block. This phenomenon may ultimately lead to either the formation of micellar aggregates or the generation of vesicles, accompanied by rearrangement of the hydrophilic and hydrophobic segments of the copolymers.

In the case of the remaining samples, namely PNVP-b-PVBu #3, #4 and #5, which contain a higher percentage of the hydrophobic PVBu block ranging from 43% to 52%, the predominance of micellar aggregates or vesicles over the simple micellar structures is clearly evident, as their percentage ranges from 65% to 80% according to CONTIN analysis. Additionally, the variation of this fraction with respect to concentration is minimal. The increased percentage of the hydrophobic PVBu block results in more stable and compact micellar cores, and in conjunction with the small sized PNVP water soluble block, it facilitates micelle–micelle interactions, ultimately favoring the formation of micellar aggregates or vesicles.

Returning to sample PNVP-b-PVBu #1, the k_D value is negative. This observation indicates that hydrodynamic interactions are predominant over thermodynamic ones. The negative k_D value further suggests that the molecular weight of the supramolecular structures is not particularly high, thereby implying that the degree of aggregation is not very high. This finding aligns more closely with the presence of vesicles in solutions, which are defined by an elevated size yet comparatively low molecular weight, as opposed to micellar aggregates.

A similar behavior is also observed in the individual distribution profiles corresponding to the two particle populations detected in the other samples by CONTIN analysis. Figure 2 displays two characteristic CONTIN plots of sample PNVP-b-PVBu #1 which exhibits one population, and of sample #2 with two populations. The rest of CONTIN plots are given in Figure S1 and Figure S2 in the Supporting Information Section, SIS.

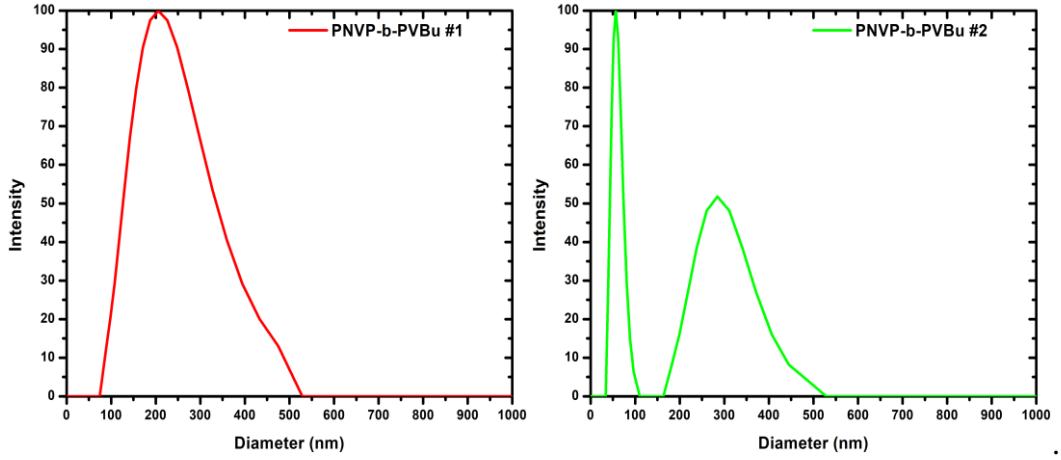

(**a**) (**b**)

Figure 2. (a) CONTIN plot of sample PNVP-b-PVBu #1 at C= 0.59 mg/mL; (b) CONTIN plot of sample PNVP-b-PVBu #2 at C= 0.289 mg/mL.

3.1.2. DLS Results for the PNVP-b-PVDc samples

As demonstrated in Table 1, all PNVP-b-PVDc samples display remarkably similar molecular weights. Consequently, the results are directly comparable in terms of molecular weight and rely exclusively on the composition of the copolymers. The results of the DLS analysis are summarized in Table 3 and characteristic DLS plots are featured in Figure 3.

 doi:10.20944/preprints202509.2475.v1

Table 3. DLS results for the PNVP-b-PVDc samples.

Sample	D_0 x10^8 (cm/s^2)	K_D	R_{h0} (nm)	$R_{h1,0}$ (nm)	$R_{h2,0}$ (nm)
PNVP-b-PVDc #1	5.84	-71	42.0	24.2	91.8
PNVP-b-PVDc #2	2.88	-502	85.0	15.6	95.4
PNVP-b-PVDc #3	3.93	-73	62.4	35.6	131.1
PNVP-b-PVDc #4	6.62	981	37.0	15.4	136.4

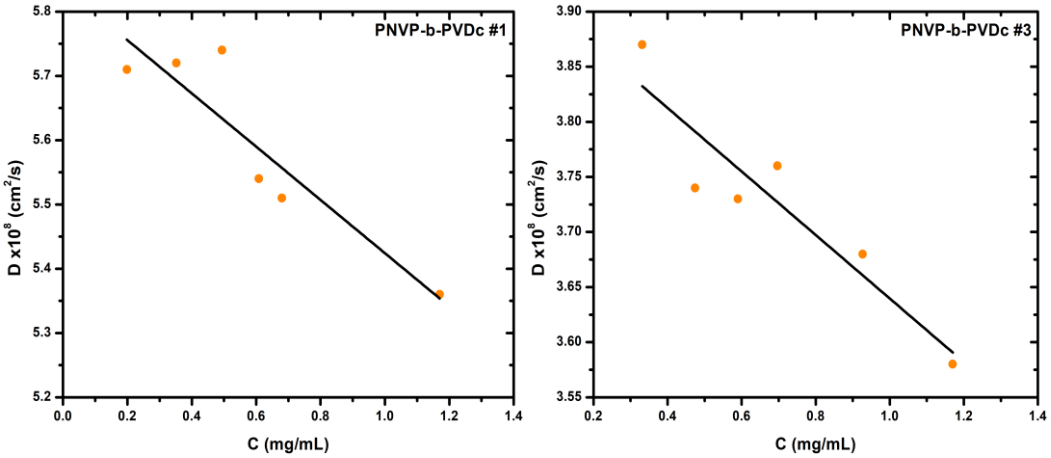

(**a**) (**b**)

Figure 3. (a) DLS plot of sample PNVP-b-PVDc #1; (b) DLS plot of sample PNVP-b-PVDc #3.

The initial observation, which is directly related to the composition of the samples, is that the overall hydrodynamic radii of the supramolecular structures formed in aqueous solution increases with increasing percentage of the hydrophobic PVDc block. Plots of the hydrodynamic radius of the two populations are displayed in Figure 4.

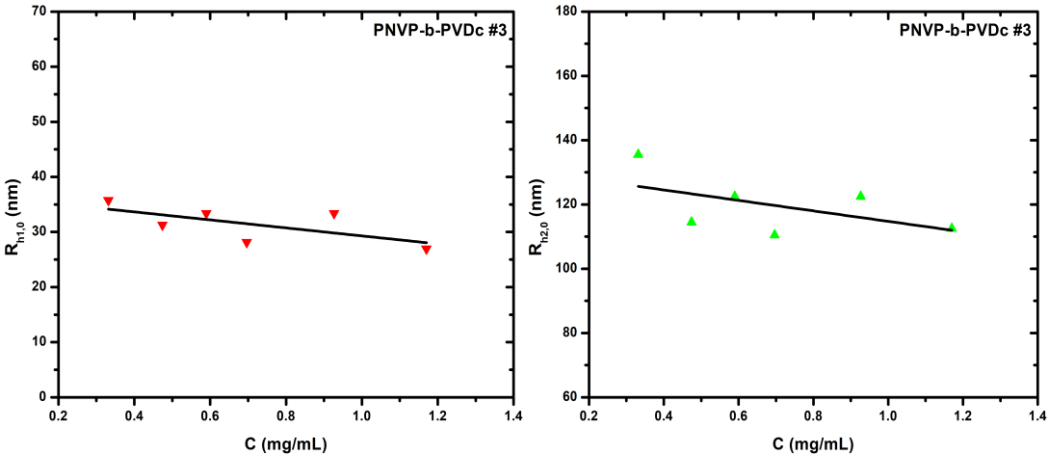

(**a**) (**b**)

Figure 4. (a) $R_{h1,0}$ vs C plot of sample PNVP-b-PVDc #3 in H_2O; (b) $R_{h2,0}$ vs C plot of sample PNVP-b-PVDc #3 in H_2O.

In addition, the CONTIN analysis reveals the presence of two distinct populations, a behavior consistent with that observed for the PNVP-b-PVBu samples, with the exception of PNVP-b-PVBu #1. The relative dimensions of the two populations further indicate that, in these samples as well, there exists an equilibrium between micelles and micellar aggregates or vesicles. In samples PNVP-b-PVDc #1, #2, and #3, the larger structures are predominant. Increasing the concentration of the solutions used for the DLS measurements reduces the contribution of simple micelles and shifts the

 doi:10.20944/preprints202509.2475.v1

equilibrium further toward the larger aggregates. The only exception to this is sample PNVP-b-PVDc #4, where the smaller micellar structure prevail, due to the fact that in this sample the percentage of the hydrophobic PVDc block is only 7%, as shown in Table 1. Representative CONTIN analysis plots are given in Figure 5 for the samples PNVP-b-PVDc #1 and #4. The CONTIN plots of the remaining two PNVP-b-PVDc samples are provided in Figure S3 in SIS.

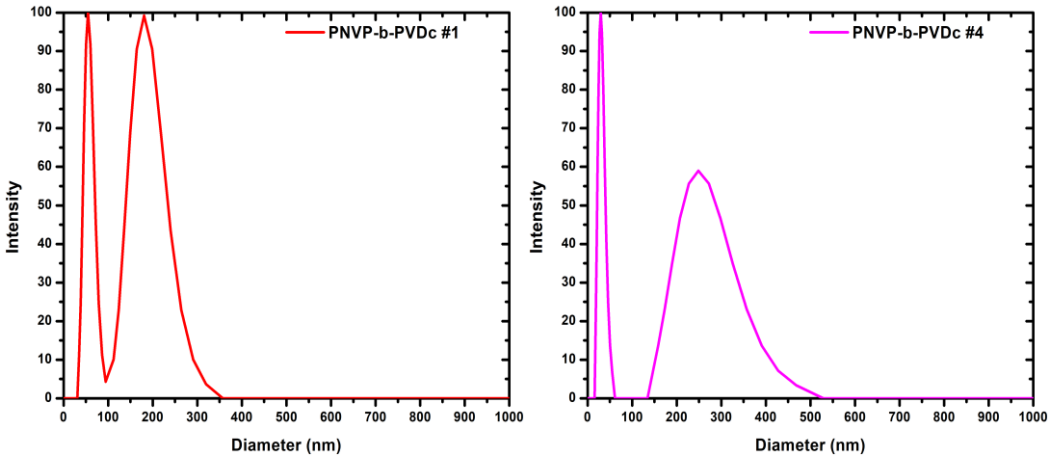

(**a**) (**b**)

Figure 5. (a) CONTIN plot of sample PNVP-b-PVDc #1 at C= 0.352 mg/mL; (b) CONTIN plot of sample PNVP-b-PVDc #4 at C= 0.925 mg/mL.

3.1.2. DLS and SLS Results for the PNVP-b-PVSt samples

As observed in the case of the amphiphilic block copolymers containing PVDc, in the last family of samples, namely PNVP-b-PVSt, all copolymers exhibit comparable molecular weights. Therefore, the results, which are presented in Table 4, again depend only on the composition of the copolymers. Example DLS plots are also provided in Figure 6.

Table 4. DLS results for the PNVP-b-PVSt samples.

Sample	D_0 x10^8 (cm/s^2)	K_D	R_{h0} (nm)
PNVP-b-PVSt #1	4.37	65.8	56.1
PNVP-b-PVSt #2	3.73	69.3	65.7
PNVP-b-PVSt #3	4.52	693.0	54.2
PNVP-b-PVSt #4	4.35	187.8	56.4
PNVP-b-PVSt #5	2.54	69.0	96.6

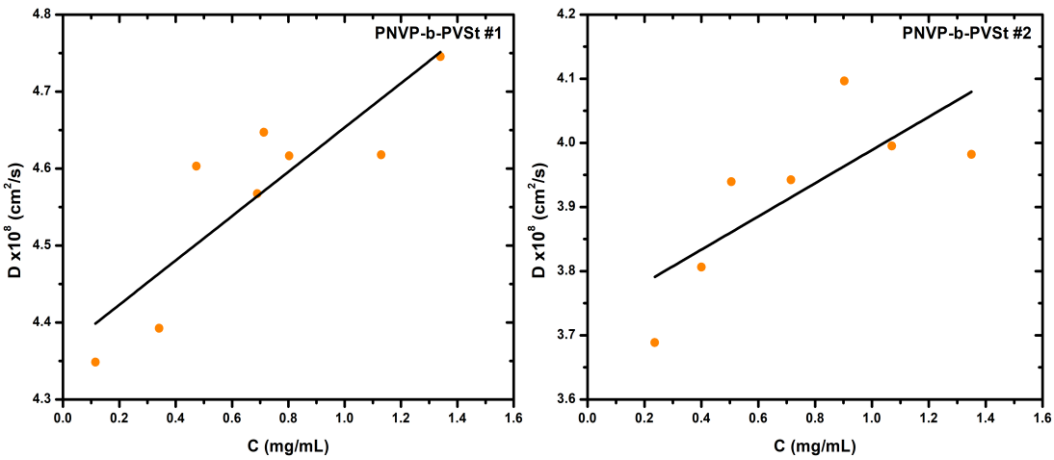

Figure 6. (a) DLS plot of sample PNVP-b-PVSt #1; (b) DLS plot of sample PNVP-b-PVSt #2.

 doi:10.20944/preprints202509.2475.v1

In contrast to all previously discussed systems, and with the sole exception of sample PNVP-b-PVBu #1, CONTIN analysis of the PNVP-b-PVSt samples reveals the presence of a single population across all concentrations of the stock solutions used for the measurements. CONTIN analysis plots are given for the sample PNVP-b-PVSt #1 and PNVP-b-PVSt #2 in Figure 7. The CONTIN analysis plots of samples PNVP-b-PVSt #3, PNVP-b-PVSt #4 and PNVP-b-PVSt #5 are included in SIS in Figure S4 and Figure S5. Taking into account the measured hydrodynamic radii, summarized in Table 4, and the relatively low molecular weights of the free chains, as shown in Table 1, it can be concluded that the structures formed in aqueous environment correspond either to micelles with a high degree of aggregation, to micellar aggregates, or to stable vesicular assemblies.

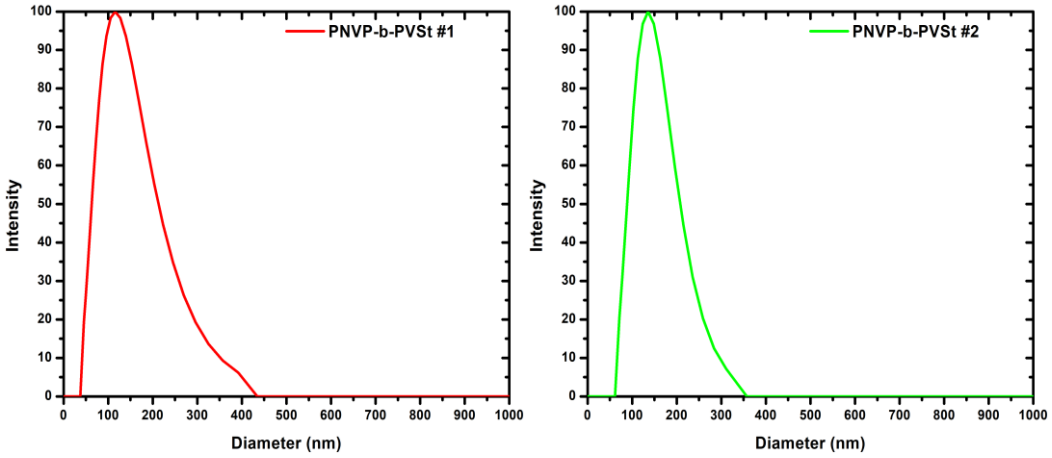

(**a**) (**b**)

Figure 7. (a) CONTIN plot of sample PNVP-b-PVSt #1 at C= 0.115 mg/mL; (b) CONTIN plot of sample PNVP-b-PVSt #2 at C= 0.236 mg/mL.

In accordance with the behavior previously observed in the PVBu- and PVDc-based amphiphilic block copolymers, the hydrodynamic radius of the supramolecular structures formed in PNVP-b-PVSt samples increases upon increasing the percentage of the hydrophobic PVSt block, most likely due to a higher degree of aggregation.

The values of the PDI for all samples exceed 0.2, indicating that the supramolecular structures formed in aqueous solution exhibit a broad size distribution. It is evident that this phenomenon can be attributed, in part, to the polydispersity of the initial copolymers. However, it is primarily attributable to the aggregation process itself. More specifically, the hydrophobic interactions within the core forming material in the PNVP-b-PVSt copolymers are stronger compared to the two other families of copolymers. The long alkyl side chains of PVSt are able to form crystalline domains leading to the formation of compact micellar cores.

In all PNVP-b-PVSt samples, the k_D values are found to be relatively low but positive due to the huge M_w of the aggregates, thus indicating that thermodynamic interactions predominate over hydrodynamic ones. As a direct consequence, and due to the reduced interactions of the polymeric system with the solvent, the corresponding A_2 values persist at sufficiently low levels.

As already mentioned, the PNVP-b-PVSt samples are the only ones that consistently exhibit a single population. Therefore, it was considered appropriate to subject these particular samples to SLS measurements as well. The detailed results are presented in Table 5, which, for convenience, also includes the information from Table 1 about the molar ratio of the hydrophobic PVSt block. Furthermore, characteristic SLS plots are presented in Figure 8.

Table 5. SLS results for the PNVP-b-PVSt samples.

Sample	PVSt [1] molar ratio (%)	$(M_w)_{micc}$ [2] (Daltons)	$(A_2)_{micc}$ [2] (cm^3mol/g^2)	Nw

 doi:10.20944/preprints202509.2475.v1

PNVP-b-PVSt #1	22	4.02 x 10^{7}	2.15 x 10^{-5}	3,828
PNVP-b-PVSt #2	39	1.18 x 10^{8}	1.65 x 10^{-5}	11,346
PNVP-b-PVSt #3	15	5.98 x 10^{7}	1.85 x 10^{-5}	5,486
PNVP-b-PVSt #4	17	4.77 x 10^{7}	1.64 x 10^{-5}	3,816
PNVP-b-PVSt #5	60	4.35 x 10^{8}	1.87 x 10^{-6}	48,333

[1] Derived by ^{1}H-NMR in $CDCl_3$. [2] Derived by SLS.

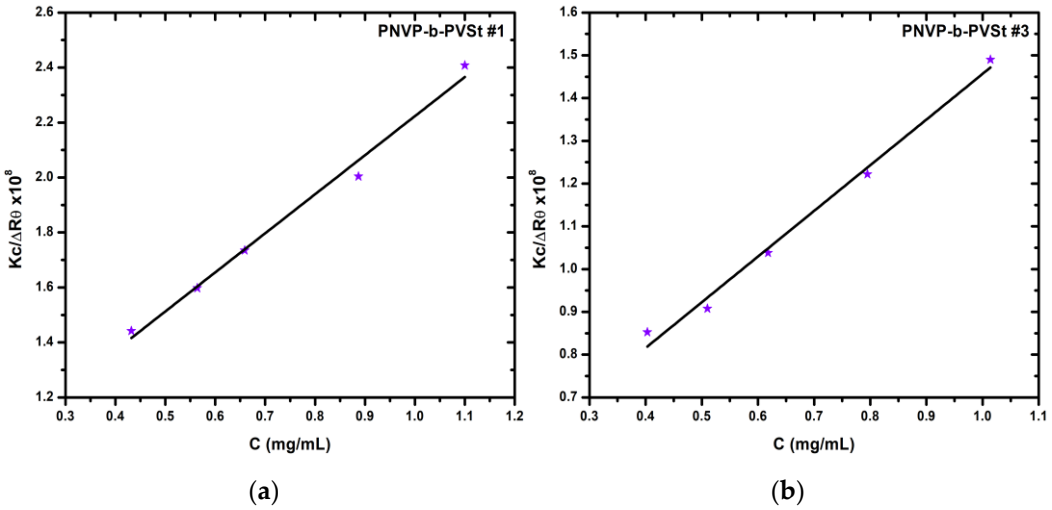

(**a**) (**b**)

Figure 8. (a) SLS plot of sample PNVP-b-PVSt #1; (b) SLS plot of sample PNVP-b-PVSt #3.

In agreement with the DLS results, the structures formed upon self-assembly of these amphiphilic block copolymers in aqueous solution are micelles characterized by an exceptionally high degree of aggregation. In general, the degree of aggregation was governed by both the block copolymer composition and the degree of polymerization. Since all samples share nearly identical molecular characteristics, the degree of association is dictated exclusively by the copolymer composition.

More specifically, as the percentage of the hydrophilic PNVP block decreases, corresponding to an increase in the percentage of the hydrophobic PVSt block, the degree of association value, Nw, rises dramatically. For instance, in PNVP-b-PVSt samples #1, #2, and #3, where the PNVP content ranges between 78 and 85%, Nw is already very high, from approximately 3,800 up to 5,500. Upon reduction of the percentage of the PNVP block to 61% in sample #4, Nw increases to about 11,000, and in sample #5, containing only 40% PNVP, Nw reaches an exceptionally high value of over 48,000. This behavior reflects the formation of a highly compact and rigid hydrophobic core, effectively minimizing the unfavorable hydrophobic–water interfacial area.

3.2. Drug Encapsulation Results

3.2.1. Encapsulation of Curcumin

The results of curcumin encapsulation within the dry cores of the micellar structures formed by the self-assembly of the PNVP-b-PVBu amphiphilic block copolymers in aqueous solution are summarized in Table 6. UV-Vis spectra of PNVP-b-PVBu samples with all concentrations of encapsulated curcumin are given in Figure S6 and Figure S7 in SIS.

Table 6. Results of curcumin encapsulation within the dry core of the micellar structures formed in aqueous solutions by the PNVP-b-PVBu samples.

Sample	Cur. [1]	A [2] (a.u.)	Pol. [3] (μg/mL)	DIF [4] (μg/mL)	LD [5] (μg/mL)	DLC (%)	DLE (%)
PNVP-b-PVBu	1%	1.85	481.20	12.60	9.19	1.91	73.01
#1	2%	1.78	670.09	14.59	8.83	1.32	60.54

 doi:10.20944/preprints202509.2475.v1

	3%	2.85	653.62	17.93	14.33	2.19	79.90
	4%	2.74	643.69	21.22	13.76	2.14	64.85
	1%	0.45	543.50	6.23	2.00	0.37	32.08
PNVP-b-PVBu #2	2%	1.57	604.45	14.17	7.75	1.28	54.72
	3%	1.85	599.34	17.42	9.19	1.53	52.75
	4%	2.55	621.73	21.75	12.79	2.06	58.80
	1%	0.38	583.23	6.33	1.64	0.28	25.90
PNVP-b-PVBu #3	2%	1.84	650.11	14.12	9.14	1.41	64.73
	3%	1.97	637.42	17.22	9.81	1.54	56.94
	4%	2.34	630.40	21.68	11.71	1.86	54.01
	1%	0.37	537.80	5.97	1.59	0.30	26.61
PNVP-b-PVBu #4	2%	1.94	632.52	14.38	9.65	1.53	67.13
	3%	1.93	619.94	17.38	9.60	1.55	55.23
	4%	2.89	638.81	22.02	14.53	2.27	65.99

[1] Concentration of the curcumin. [2] Absorbance. [3] Concentration of the polymer stock solutions in H_2O. [4] Concentration of the drug in feed. [5] Concentration of the loaded drug.

As demonstrated in Table 6, the encapsulation efficiency is found to be noteworthy, with the DLE values attaining a maximum of 80%. As might have been anticipated, sample PNVP-b-PVBu #1, which contains the highest amount of the hydrophobic PVBu block and exhibits a single population of micellar aggregates, as evidenced by the DLS results in Table 2, shows the highest encapsulation capacity.

Among the three remaining samples, PNVP-b-PVBu #2 may demonstrate a slightly higher encapsulation performance due to the larger hydrodynamic radius of its second micellar population, however, this sample, along with samples PNVP-b-PVBu #3 and #4, display a very similar behavior overall. This observation is consistent with the DLS results presented in Table 2, given the coexistence of micelles with clusters or micellar aggregates in all three cases, as previously discussed.

Overall, the observed behavior is in accordance with the anticipated trend, whereby the percentage of curcumin encapsulation increases as the feed concentration increases, as demonstrated by the increase in DLC values. However, in case of DLE, after an initial rise, DLE values appear to level off, reaching a plateau with nearly constant values.

The corresponding results for the PNVP-b-PVDc samples are presented in Table 7 and the respected UV-Vis spectra are featured in Figure S8 and Figure S9 in SIS. The values of DLC and DLE are satisfactory and quite comparable to those of the PNVP-b-PVBu samples, which is consistent with the similar core sizes of the micellar structures formed through their self-assembly in aqueous environments, as also indicated by the hydrodynamic radii of the second micellar populations, summarized in Tables 2 and 3, for the PNVP-b-PVBu samples and the PNVP-b-PVDc samples, respectively. Nevertheless, the increase in the hydrophobic segment length of the n-alkyl side chain in PVDc compared to that of PVBu results in a rise in the DLE values, most likely due to stronger interactions with curcumin.

Table 7. Results of curcumin encapsulation within the dry core of the micellar structures formed in aqueous solutions by the PNVP-b-PVDc samples.

Sample	Cur. [1]	A [2] (a.u.)	Pol. [3] (μg/mL)	DIF [4] (μg/mL)	LD [5] (μg/mL)	DLC (%)	DLE (%)
	1%	0.61	684.13	6.18	4.82	0.71	78.05
PNVP-b-PVDc #1	2%	2.12	746.70	13.79	2.82	0.38	20.46
	3%	2.64	765.59	17.73	10.58	1.38	59.64
	4%	1.92	767.62	21.11	13.25	1.73	62.77
PNVP-b-PVDc #2	1%	0.73	601.64	6.37	9.55	1.59	49.88
	2%	2.17	668.63	13.92	3.44	0.51	24.69

 doi:10.20944/preprints202509.2475.v1

	3%	2.68	676.55	17.69	10.83	1.60	61.25
	4%	1.69	641.88	20.09	13.45	2.10	66.96
PNVP-b-PVDc #3	1%	0.93	615.39	6.91	8.37	1.36	21.18
	2%	2.08	619.55	14.25	4.46	0.72	31.33
	3%	2.52	592.96	17.34	10.37	1.75	59.81
	4%	2.19	624.96	21.81	12.63	2.02	57.93
PNVP-b-PVDc #4	1%	0.86	560.35	66.07	10.94	1.95	65.54
	2%	1.96	552.45	13.03	4.11	0.74	31.50
	3%	2.21	546.12	16.24	9.76	1.79	60.06
	4%	2.81	544.62	19.41	11.04	2.03	56.87

[1] Concentration of the curcumin. [2] Absorbance. [3] Concentration of the polymer stock solutions in H_2O. [4] Concentration of the drug in feed. [5] Concentration of the loaded drug.

More specifically, in the case of the PNVP-b-PVDc amphiphilic block copolymers, for samples #2 and #3, the DLE values increase with increasing concentration of curcumin in feed. On the other hand, for samples #3 and #4, as the concentration of curcumin in feed increases from C_3 to C_4, a slight decrease in DLE values is observed.

This phenomenon was also noted to a smaller extent to the PNVP-b-PVBu samples and may be attributed to the fact that at higher concentrations, curcumin tends to form aggregates and precipitate. Such behavior is not uncommon for organic dyes, where molecular aggregation in solution frequently occurs, notably in the form of H-aggregates and J-aggregates, particularly at elevated dye concentrations. [34–37] It is characteristic that dye aggregates do not exhibit the same absorption maximum wavelength as the individual dye molecules, due to slight modifications of the conjugated double-bond system within the aggregate compared to the isolated chromophore. Consequently, in some cases, anomalous absorption behavior is observed in the visible region as a function of the dye concentration in the measured solution.

The investigation of curcumin encapsulation within the micellar structures of the PNVP-b-PVSt amphiphilic block copolymer samples yielded promising results, as summarized in Table 8. The characteristic UV-Vis spectra are all displayed in Figure S10 and Figure S11 in SIS. The hydrophobic drug was successfully incorporated to a satisfactory extent, with all samples exhibiting DLE values above 40%. Similar to the case of the PNVP-b-PVBu samples, the DLE initially tends to increase until it reaches a plateau with nearly constant values. However, for the PNVP-b-PVSt samples, there is a more specific explanation. As previously mentioned, the long alkyl side chains of PVSt are capable of forming crystalline domains, which reduce the capacity of the compact core, thereby limiting the available space for the encapsulation of higher amounts of curcumin.

Table 8. Results of curcumin encapsulation within the dry core of the micellar structures formed in aqueous solutions by the PNVP-b-PVSt samples.

Sample	Cur. [1]	A [2] (a.u.)	Pol. [3] (μg/mL)	DIF [4] (μg/mL)	LD [5] (μg/mL)	DLC (%)	DLE (%)
PNVP-b-PVSt #1	1%	0.63	553.69	6.20	2.92	0.53	47.17
	2%	1.48	570.94	13.26	7.29	1.28	54.98
	3%	1.61	522.77	14.91	7.96	1.52	53.36
	4%	2.24	567.39	19.22	11.19	1.97	58.25
PNVP-b-PVSt #2	1%	0.67	567.63	6.25	3.13	0.55	50.04
	2%	1.74	571.86	12.87	8.63	1.51	67.01
	3%	1.95	580.85	16.02	9.70	1.67	60.59
	4%	2.38	577.08	19.90	11.91	2.06	59.87
PNVP-b-PVSt #3	1%	0.68	554.27	6.15	3.18	0.57	51.70
	2%	1.57	574.55	12.91	7.75	1.35	60.06
	3%	1.86	574.47	16.01	9.24	1.61	57.74

 doi:10.20944/preprints202509.2475.v1

	4%	2.51	591.43	19.06	12.58	2.13	65.99
PNVP-b-PVSt #4	1%	0.48	554.60	5.42	2.15	0.39	39.72
	2%	1.48	560.06	11.74	7.29	1.30	62.12
	3%	2.04	558.56	14.81	10.17	1.82	68.64
	4%	2.19	566.32	18.06	10.94	1.93	60.55

[1] Concentration of the curcumin. [2] Absorbance. [3] Concentration of the polymer stock solutions in H_2O. [4] Concentration of the drug in feed. [5] Concentration of the loaded drug.

3.2.2. Encapsulation of Indomethacin

In addition to the encapsulation of curcumin, the encapsulation of the hydrophobic drug indomethacin within the dry cores of the micellar structures formed by the self-assembly of the PNVP-b-PVEs amphiphilic block copolymers in aqueous solution, was also investigated. The results of the encapsulation of indomethacin, into the PNVP-b-PVBu samples are presented in Table 9. As mentioned, UV-Vis spectroscopy was utilized for the quantitative determination of indomethacin in the solutions in which its encapsulation was attempted, therefore, in SIS Figure S12 exhibits the UV-Vis spectra of indomethacin with various concentrations and the calibration curve for indomethacin at 320 nm. Figure 9 presents UV-Vis spectra of sample PNVP-b-PVBu #2 and PNVP-b-PVBu #5, respectively, with all three different concentrations of encapsulated indomethacin combined, while the UV-Vis spectra of the remaining PNVP-b-PVBu samples are included in Figure S13 and Figure S14 in SIS.

Table 9. Results of indomethacin encapsulation within the dry core of the micellar structures formed in aqueous solutions by the PNVP-b-PVBu samples.

Sample	Ind. [1] (w/w)	A [2] (a.u.)	Pol. [3] (μg/mL)	DIF [4] (μg/mL)	LD [5] (μg/mL)	DLC (%)	DLE (%)
PNVP-b-PVBu #1	10%	0.32	178.34	17.16	12.53	7.02	73.00
	15%	0.69	169.51	24.48	28.93	17.07	118.17
	20%	0.80	168.85	34.39	33.98	20.13	98.83
PNVP-b-PVBu #2	10%	0.27	168.70	15.97	10.56	6.26	66.16
	15%	0.37	164.15	25.65	14.93	9.09	58.21
	20%	0.45	166.63	33.01	18.24	10.95	55.26
PNVP-b-PVBu #3	10%	0.32	180.86	16.18	12.55	6.94	77.58
	15%	0.40	182.12	25.69	16.12	8.85	62.76
	20%	0.61	187.77	34.82	25.70	13.69	73.82
PNVP-b-PVBu #4	10%	0.30	171.48	16.54	11.90	6.94	71.95
	15%	0.32	173.91	23.46	42.45	7.16	53.07
	20%	0.56	173.42	32.31	23.32	13.45	72.18
PNVP-b-PVBu #5	10%	0.30	165.14	15.93	11.75	7.11	73.73
	15%	0.43	165.03	24.82	17.41	10.55	70.13
	20%	0.61	164.20	35.00	25.46	15.51	72.75

[1] Concentration of the indomethacin solutions in THF (w/w indomethacin/polymer). [2] Absorbance. [3] Concentration of the polymer stock solutions in H_2O. [4] Concentration of the drug in feed. [5] Concentration of the loaded drug.

 doi:10.20944/preprints202509.2475.v1

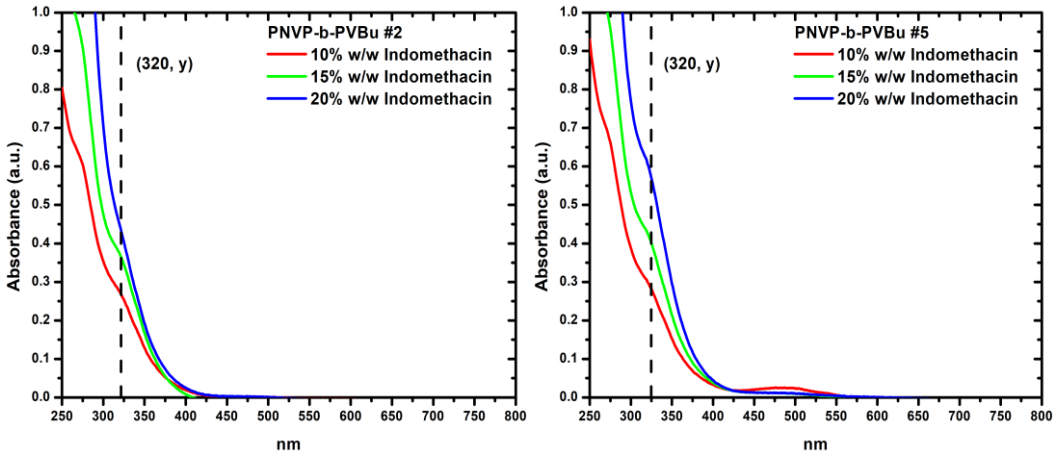

(**a**) (**b**)

Figure 9. (a) UV-Vis spectra of PNVP-b-PVBu #2 with all concentrations of encapsulated indomethacin; (b) UV-Vis spectra of PNVP-b-PVBu #5 with all concentrations of encapsulated indomethacin.

Sample PNVP-b-PVBu #1, which, as shown in its composition in Table 1, contains the highest percentage of the hydrophobic PVBu block, displays the highest DLC and DLE values for the encapsulation of indomethacin, consistent with the trend previously observed for curcumin. Remarkably, the addition of up to 20% w/w indomethacin leads to nearly quantitative encapsulation. In contrast to sample #1, PNVP-b-PVBu #2 shows the lowest DLC and DLE values, precisely because, as indicated in Table 1, it contains the lowest percentage of the hydrophobic PVBu block.

The three remaining samples, PNVP-b-PVBu #3, #4 and #5, which, possess similar compositions and intermediate percentages of the hydrophobic PVBu block relative to the two extreme cases of samples #1 and #2, exhibit comparable behaviors and DLC/DLE values, falling between those observed for samples #1 and #2, as expected.

The results regarding the encapsulation of indomethacin within the PNVP-b-PVDc samples are summarized in Table 10 and characteristic UV-Vis spectra are given in Figure 10 with the rest of UV-Vis spectra being given in Figure S15 in SIS.

Table 10. Results of indomethacin encapsulation within the dry core of the micellar structures formed in aqueous solutions by the PNVP-b-PVDc samples.

Sample	Ind. [1] (w/w)	A [2] (a.u.)	Pol. [3] (μg/mL)	DIF [4] (μg/mL)	LD [5] (μg/mL)	DLC (%)	DLE (%)
PNVP-b-PVDc #1	10%	0.24	73.25	17.63	9.18	12.53	52.05
	15%	0.32	94.67	16.09	12.57	13.28	78.09
	20%	0.49	98.63	19.59	20.06	20.34	102.38
PNVP-b-PVDc #2	10%	0.39	95.43	10.15	15.66	16.41	154.22
	15%	0.55	98.59	15.65	22.65	22.98	144.74
	20%	0.69	101.96	19.60	29.14	28.58	148.66
PNVP-b-PVDc #3	10%	0.20	107.78	10.36	7.46	6.92	72.02
	15%	0.33	109.01	17.25	12.88	11.82	74.97
	20%	0.48	105.61	19.48	19.90	18.84	102.16
PNVP-b-PVDc #4	10%	0.26	97.04	10.24	10.00	10.31	97.64
	15%	0.31	94.03	16.07	11.98	12.75	74.59
	20%	0.52	92.95	19.92	21.67	23.32	108.77

[1] Concentration of the indomethacin solutions in THF (w/w indomethacin/polymer). [2] Absorbance. [3] Concentration of the polymer stock solutions in H_2O. [4] Concentration of the drug in feed. [5] Concentration of the loaded drug.

 doi:10.20944/preprints202509.2475.v1

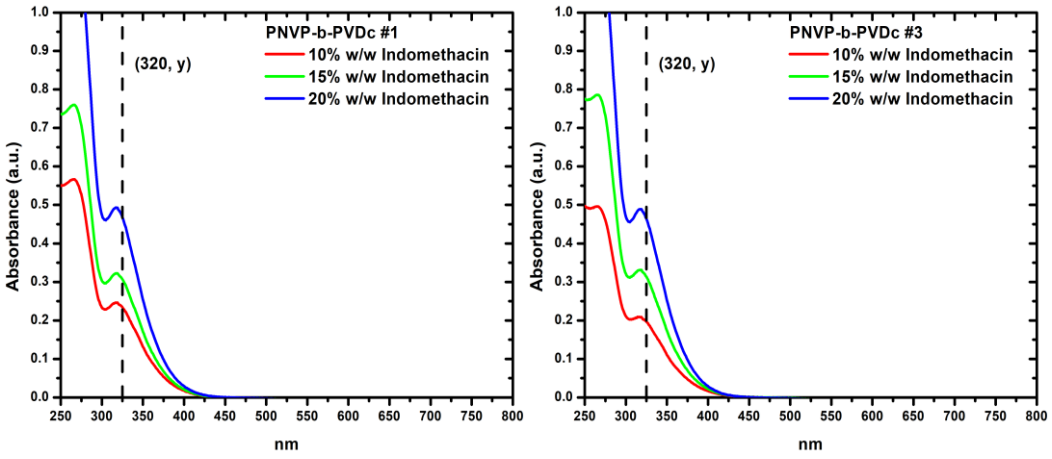

(**a**) (**b**)

Figure 10. (a) UV-Vis spectra of PNVP-b-PVDc #1 with all concentrations of encapsulated indomethacin (b) UV-Vis spectra of PNVP-b-PVDc #3 with all concentrations of encapsulated indomethacin.

The encapsulation results of indomethacin in the PNVP-b-PVDc samples are remarkably high. The DLC values closely match the respective feed concentrations of indomethacin, while the DLE demonstrates that, in the vast majority of samples, the incorporation of indomethacin into the dry micellar core is essentially quantitative. These findings highlight that indomethacin is more efficiently accommodated within the micelles compared to curcumin. In the case of PNVP-b-PVDc, the encapsulation efficiency surpasses that of the PNVP-b-PVBu samples, which can be attributed to the longer n-alkyl hydrophobic side chains of PVDc that promote stronger hydrophobic interactions with the hydrophobic drug molecules.

Finally, the encapsulation performance of indomethacin within the PNVP-b-PVSt samples is highlighted in Table 11 accompanied with UV-Vis spectra in Figure 11. The last UV-Vis spectra are placed in Figure S16 and Figure S17 in SIS.

Table 11. Results of indomethacin encapsulation within the dry core of the micellar structures formed in aqueous solutions by the PNVP-b-PVSt samples.

Sample	Ind. [1] (w/w)	A [2] (a.u.)	Pol. [3] (μg/mL)	DIF [4] (μg/mL)	LD [5] (μg/mL)	DLC (%)	DLE (%)
PNVP-b-PVSt #1	10%	0.39	165.90	15.95	15.66	9.44	98.19
	15%	0.46	164.14	23.65	18.75	11.42	79.26
	20%	0.55	166.71	38.53	22.68	13.60	58.87
PNVP-b-PVSt #2	10%	0.73	32.93	3.27	31.06	9.43	94.9
	15%	0.36	166.27	24.02	14.17	8.52	58.98
	20%	0.65	166.17	33.13	27.49	16.54	82.98
PNVP-b-PVSt #3	10%	0.45	165.82	18.98	18.22	10.99	96.01
	15%	0.55	181.78	27.56	22.82	12.55	82.80
	20%	0.62	168.32	33.06	25.75	15.30	77.90
PNVP-b-PVSt #4	10%	0.41	172.92	16.89	16.71	9.66	98.93
	15%	0.51	167.90	24.12	21.07	12.55	87.33
	20%	0.55	171.99	35.92	22.74	13.22	63.30
PNVP-b-PVSt #5	10%	0.84	157.27	16.47	35.96	22.86	218.31
	15%	0.84	152.17	25.01	35.64	23.42	142.47
	20%	0.90	150.52	33.06	38.35	25.48	116.01

[1] Concentration of the indomethacin solutions in THF (w/w indomethacin/polymer). [2] Absorbance. [3] Concentration of the polymer stock solutions in H_2O. [4] Concentration of the drug in feed. [5] Concentration of the loaded drug.

 doi:10.20944/preprints202509.2475.v1

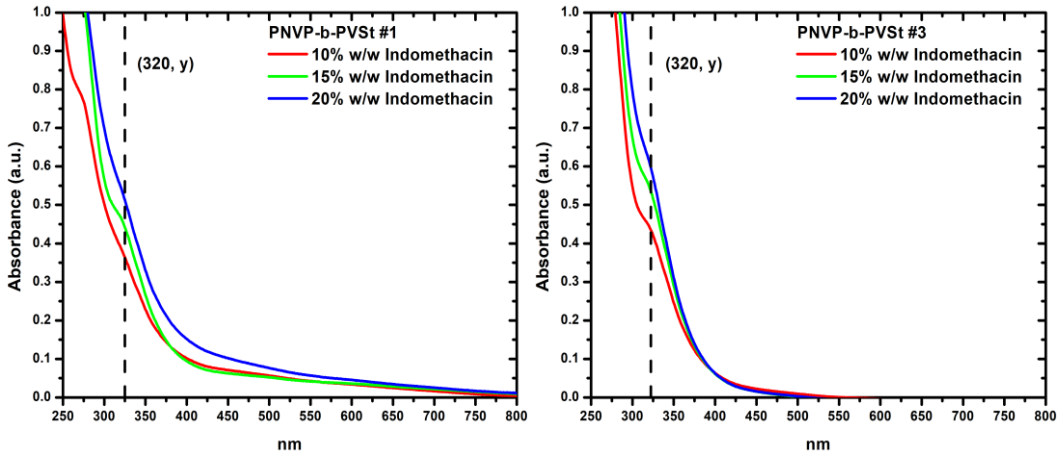

(**a**) (**b**)

Figure 11. (a) UV-Vis spectra of PNVP-b-PVSt #1 with all concentrations of encapsulated indomethacin (b) UV-Vis spectra of PNVP-b-PVSt #3 with all concentrations of encapsulated indomethacin.

All PNVP-b-PVSt samples exhibit consistent behavior. At an indomethacin feed concentration of 10% w/w indomethacin/polymer, encapsulation is nearly quantitative, with DLE values approaching 100%. However, further increases in feed concentration lead to a sharp decline in DLE values. This behavior contrasts with that of PNVP-b-PVBu and PNVP-b-PVDc, yet it can be fully explained by the nature of the micelles. In PNVP-b-PVDc samples, longer n-alkyl side chains enhance loading capacity and efficiency, compared to PNVP-b-PVBu samples, due to the amorphous micellar core, which provides ample space for drug incorporation. In PNVP-b-PVSt samples, however, the PVSt block crystallizes, significantly reducing the available core volume. Consequently, full encapsulation is achieved only up to 10% w/w, corresponding to the observed DLC values, while beyond this threshold, the core becomes saturated, preventing further indomethacin loading, which is clearly reflected in the steep drop of DLE at higher feed concentrations.

4. Conclusions

Water acts as a selective solvent for the PNVP-b-PVEs amphiphilic block copolymers, enabling their self-assembly into micellar structures upon dissolution. In the cases of PNVP-b-PVBu and PNVP-b-PVDc copolymers, where k_D values are negative, interparticle hydrodynamic interactions prevail, whereas in the case of PNVP-b-PVSt samples, self-assembly in aqueous media is a thermodynamically driven process, as indicated by the positive k_D values. The investigation of the self-assembly of PNVP-b-PVEs, which differ in the length of their n- alkyl side chains, further demonstrated the impact of this parameter on their micellization behavior. Specifically, PNVP-b-PVBu and PNVP-b-PVDc samples, bearing short and medium-length side chains, respectively, exhibited an equilibrium between two populations of micelles and micelle aggregates or vesicles, whereas in the PNVP-b-PVSt samples, with the longest aliphatic side chain, only a single population was detected. Within each copolymer family, the effect of composition on the morphology of the formed structures was also evident. In all cases, increasing the percentage of the hydrophobic PVE block resulted in an enlargement of the micellar core size and, consequently, an increase in the hydrodynamic radius. Encapsulation of hydrophobic bioactive molecules within the micellar cores was successful for both curcumin and indomethacin. In practice, these amphiphilic block copolymers proved more effective in encapsulating indomethacin compared to curcumin. Copolymer composition was identified as the key parameter for enhancing loading capacity and efficiency, as higher hydrophobic PVE percentage consistently led to increased DLC and DLE values due to enlargement of the hydrodynamic radius. Comparison among the three PNVP-b-PVEs copolymer families revealed that PNVP-b-PVBu samples displayed the highest loading capacity and efficiency. This outcome is attributed to the medium-length n-alkyl side chain, which promoted swelling of the

 doi:10.20944/preprints202509.2475.v1

dry core and remained amorphous, thus providing additional free volume for drug incorporation. By contrast, PNVP-b-PVBu copolymers with shorter side chains offered limited internal space, while PNVP-b-PVSt copolymers exhibited a plateau in loading capacity (ca. 10% DLC). The latter limitation arises from the crystallization of the longest alkyl side chains, which restricts the available core volume. In summary, the morphology, size, and stability of the self-assembled nanostructures, combined with the remarkably high DLC and DLE values, particularly in the case of indomethacin, strongly suggest that the amphiphilic block copolymers investigated in this study demonstrate significant potential as carriers for drug delivery applications.

Supplementary Materials: The following supporting information can be downloaded at the website of this paper posted on Preprints.org, Figure S1. (a) CONTIN plot of sample PNVP-b-PVBu #3 at C= 0.093 mg/mL; (b) CONTIN plot of sample PNVP-b-PVBu #4 at C= 0.758 mg/mL.; Figure S2: CONTIN plot of sample PNVP-b-PVBu #5 at C= 0.095 mg/mL.; Figure S3: (a) CONTIN plot of sample PNVP-b-PVDc #2 at C= 0.659 mg/mL; (b) CONTIN plot of sample PNVP-b-PVDc #3 at C= 0.59 mg/mL.; Figure S4: (a) CONTIN plot of sample PNVP-b-PVSt #3 at C= 0.257 mg/mL; (b) CONTIN plot of sample PNVP-b-PVSt #4 at C= 0.081 mg/mL.; Figure S5: CONTIN plot of sample PNVP-b-PVSt #3 at C= 0.054 mg/mL.; Figure S6: (a) UV-Vis spectra of PNVP-b-PVBu #1 with all concentrations of encapsulated curcumin; (b) UV-Vis spectra of PNVP-b-PVBu #2 with all concentrations of encapsulated curcumin.; Figure S7; (a) UV-Vis spectra of PNVP-b-PVBu #3 with all concentrations of encapsulated curcumin; (b) UV-Vis spectra of PNVP-b-PVBu #4 with all concentrations of encapsulated curcumin.; Figure S8; (a) UV-Vis spectra of PNVP-b-PVDc #1 with all concentrations of encapsulated cur-cumin; (b) UV-Vis spectra of PNVP-b-PVDc #2 with all concentrations of encapsulated curcumin.; Figure S9: (a) UV-Vis spectra of PNVP-b-PVDc #3 with all concentrations of encapsulated cur-cumin; (b) UV-Vis spectra of PNVP-b-PVDc #4 with all concentrations of encapsulated curcumin.; Figure S10: (a) UV-Vis spectra of PNVP-b-PVSt #1 with all concentrations of encapsulated curcumin; (b) UV-Vis spectra of PNVP-b-PVSt #2 with all concentrations of encapsulated curcumin.; Figure S11: (a) UV-Vis spectra of PNVP-b-PVSt #3 with all concentrations of encapsulated curcumin; (b) UV-Vis spectra of PNVP-b-PVSt #4 with all concentrations of encapsulated curcumin.; Figure S12: (a) UV-Vis spectra of indomethacin with various concentrations; (b) Calibration curve for indomethacin at 320 nm.; Figure S13: (a) UV-Vis spectra of PNVP-b-PVBu #1 with all concentrations of encapsulated indomethacin; (b) UV-Vis spectra of PNVP-b-PVBu #3 with all concentrations of encapsulated indomethacin.; Figure S14: UV-Vis spectra of PNVP-b-PVBu #4 with all concentrations of encapsulated indomethacin.; Figure S15: (a) UV-Vis spectra of PNVP-b-PVDc #2 with all concentrations of encapsulated indomethacin; (b) UV-Vis spectra of PNVP-b-PVDc #4 with all concentrations of encapsulated indomethacin.; Figure S16: (a) UV-Vis spectra of PNVP-b-PVSt #2 with all concentrations of encapsulated indomethacin; (b) UV-Vis spectra of PNVP-b-PVSt #4 with all concentrations of encapsulated indomethacin.; Figure S17: UV-Vis spectra of PNVP-b-PVSt #5 with all concentrations of encapsulated indomethacin.

Author Contributions: Conceptualization, M.P.; methodology, N.V.P. and N.R.; investigation, N.V.P. (DLS, SLS, indomethacin encapsulation), A.M.G. (DLS, SLS), A.A. (DLS), A.B. (DLS), T.P.P (investigation) and N.R. (curcumin encapsulation); writing—original draft preparation, N.V.P.; writing—review and editing, M.P.; visualization, N.V.P.; supervision, M.P.; project administration, M.P.; funding acquisition, N.R. All authors have read and agreed to the published version of the manuscript.

Funding: This research was co-funded by Greece and the European Union (European Social Fund-ESF) through the Operational Program «Human Resources Development, Education and Lifelong Learning» in the context of the project “Strengthening Human Resources Research Potential via Doctorate Research” (MIS-5000432), implemented by the State Scholarships Foundation (IKY).

Institutional Review Board Statement: Not applicable.

Data Availability Statement: The original contributions presented in this study are included in the article/Supplementary Materials. Further inquiries can be directed to the corresponding author.

Conflicts of Interest: The authors declare no conflicts of interest.

 doi:10.20944/preprints202509.2475.v1

References

1. Xie, B.; Liu, Y.; Li, X.; Yang, P.; He, W. Solubilization techniques used for poorly water-soluble drugs. *Acta Pharm. Sin. B* **2024**, *14*, 4683–4716. https://doi.org/10.1016/j.apsb.2024.08.027
2. Williams, H.D.; Trevaskis, N.L.; Charman, S.A.; Shanker, R.M.; Charman, W.N.; Pouton, C.W.; Porter, C.J.H. Strategies to Address Low Drug Solubility in Discovery and Development. *Pharmacol. Rev.* **2013**, *65*, 315–499. https://doi.org/10.1124/pr.112.005660
3. Kawabata, Y.; Wada, K.; Nakatani, M.; Yamada, S.; Onoue, S. Formulation Design for Poorly Water-Soluble Drugs Based on Biopharmaceutics Classification System: Basic Approaches and Practical Applications. *Int. J. Pharm.* **2011**, *420*, 1–10. https://doi.org/10.1016/j.ijpharm.2011.08.032
4. Bhalani, D.V.; Nutan, B.; Kumar, A.; Chandel, A.K.S. Bioavailability Enhancement Techniques for Poorly Aqueous Soluble Drugs and Therapeutics. *Biomedicines* **2022**, *10*, 2055. https://doi.org/10.3390/biomedicines10092055
5. Boyd, B.J.; Bergström, C.A.S.; Vinarov, Z.; Kuentz, M.; Brouwers, J.; Augustijns, P.; Brandl, M.; Bernkop-Schnürch, A.; Shrestha, N.; Préat, V.; Müllertz, A.; Bauer-Brandl, A.; Jannin, V. Successful Oral Delivery of Poorly Water-Soluble Drugs Both Depends on the Intraluminal Behavior of Drugs and of Appropriate Advanced Drug Delivery Systems. *Eur. J. Pharm. Sci.* **2019**, *137*, 104967. https://doi.org/10.1016/j.ejps.2019.104967
6. Stielow, M.; Witczyńska, A.; Kubryń, N.; Fijałkowski, Ł.; Nowaczyk, J.; Nowaczyk, A. The Bioavailability of Drugs—The Current State of Knowledge. *Molecules* **2023**, *28*, 8038. https://doi.org/10.3390/molecules28248038
7. Kalepu, S.; Nekkanti, V. Insoluble Drug Delivery Strategies: Review of Recent Advances and Business Prospects. *Acta Pharm. Sin. B* **2015**, *5*, 442–453. https://doi.org/10.1016/j.apsb.2015.07.003
8. Hwang, D.; Ramsey, J.D.; Kabanov, A.V. Polymeric Micelles for the Delivery of Poorly Soluble Drugs: From Nanoformulation to Clinical Approval. *Adv. Drug Deliv. Rev.* **2020**, *156*, 80–118. https://doi.org/10.1016/j.addr.2020.09.009
9. Kuperkar, K.; Patel, D.; Atanase, L.I.; Bahadur, P. Amphiphilic Block Copolymers: Their Structures, and Self-Assembly to Polymeric Micelles and Polymersomes as Drug Delivery Vehicles. *Polymers* **2022**, *14*, 4702. https://doi.org/10.3390/polym14214702
10. Negut, I.; Bita, B. Polymeric Micellar Systems—A Special Emphasis on "Smart" Drug Delivery. *Pharmaceutics* **2023**, *15*, 976. https://doi.org/10.3390/pharmaceutics15030976
11. Cabral, H.; Miyata, K.; Osada, K.; Kataoka, K. Block Copolymer Micelles in Nanomedicine Applications. *Chem. Rev.* **2018**, *118*, 6844–6892. https://doi.org/10.1021/acs.chemrev.8b00199
12. Othman, R.S.; Zarei, S.; Haghighat, H.R.; Taromi, A.A.; Khonakdar, H.A. Recent Advances in Smart Polymeric Micelles for Targeted Drug Delivery. *Polym. Adv. Technol.* **2025**, *36*, e70180. https://doi.org/10.1002/pat.70180
13. Chroni, A.; Chrysostomou, V.; Skandalis, A.; Pispas, S. Drug Delivery: Hydrophobic Drug Encapsulation into Amphiphilic Block Copolymer Micelles. In Supramolecules in Drug Discovery and Drug Delivery; Mavromoustakos, T., Tzakos, A.G., Durdagi, S., Eds.; Methods in Molecular Biology; Humana: New York, NY, USA, **2021**; Volume 2207, pp. 71–85. https://doi.org/10.1007/978-1-0716-0920-0_6
14. Zheng, B.; McClements, D.J. Formulation of More Efficacious Curcumin Delivery Systems Using Colloid Science: Enhanced Solubility, Stability, and Bioavailability. *Molecules* **2020**, *25*, 2791. https://doi.org/10.3390/molecules25122791
15. Pacifici, G.M. Clinical Pharmacology of Indomethacin in Preterm Infants: Implications in Patent Ductus Arteriosus Closure. Pediatr. *Drugs* **2013**, *15*, 363–376. https://doi.org/10.1007/s40272-013-0031-7
16. Kunnumakkara, A.B.; Hegde, M.; Parama, D.; Girisa, S.; Kumar, A.; Daimary, U.D.; Garodia, P.; Yenisetti, S.C.; Oommen, O.V.; Aggarwal, B.B. Role of Turmeric and Curcumin in Prevention and Treatment of Chronic Diseases: Lessons Learned from Clinical Trials. *ACS Pharmacol. Transl. Sci.* **2023**, *6*, 447–518. https://doi.org/10.1021/acsptsci.2c00012
17. Sarkis, N.; Sawan, A. Method Development for Simultaneously Determining Indomethacin and Nicotinamide in New Combination in Oral Dosage Formulations and Co-Amorphous Systems Using Three

UV Spectrophotometric Techniques. *Int. J. Anal. Chem.* **2024**, *2024*, 2035824. https://doi.org/10.1155/2024/2035824

18. Roka, N.; Kokkorogianni, O.; Kontoes-Georgoudakis, P.; Choinopoulos, I.; Pitsikalis, M. Recent Advances in the Synthesis of Complex Macromolecular Architectures Based on Poly(N-vinyl pyrrolidone) and the RAFT Polymerization Technique. *Polymers* **2022**, *14*(4), 701. https://doi.org/10.3390/polym14040701
19. Berger, M.; Toussaint, F.; Ben Djemaa, S.; Laloy, J.; Pendeville, H.; Evrard, B.; Jerôme, C.; Lechanteur, A.; Mottet, D.; Debuigne, A.; et al. Poly(vinyl pyrrolidone) derivatives as PEG alternatives for stealth, non-toxic and less immunogenic siRNA-containing lipoplex delivery. *J. Control. Release* **2023**, *361*, 87–101. https://doi.org/10.1016/j.jconrel.2023.07.031
20. Liu, Y.; Luo, X.; Xu, X.; Gao, N.; Liu, X. Preparation, characterization and in vivo pharmacokinetic study of PVP-modified oleanolic acid liposomes. *Int. J. Pharm.* **2017**, *517*, 1–7. https://doi.org/10.1016/j.ijpharm.2016.11.056
21. Rinno, H. Poly(vinyl esters). In Ullmann's Encyclopedia of Industrial Chemistry; Wiley-VCH Verlag GmbH & Co. KGaA: Weinheim, Germany, **2000**; Volume 28, pp. 469–479. https://doi.org/10.1002/14356007.a22_001
22. Yamada, K.; Nakano, T.; Okamoto, Y. Synthesis of syndiotactic poly(vinyl alcohol) from fluorine-containing vinyl esters. *Polym. J.* **1998**, *42*, 9679–9686. https://doi.org/10.1295/polymj.30.641
23. Perinelli, D.R.; Cespi, M.; Lorusso, N.; Palmieri, G.F.; Bonacucina, G.; Blasi, P. Surfactant Self-Assembling and Critical Micelle Concentration: One Approach Fits All? *Langmuir* **2020**, *36*, 5745–5753. https://doi.org/10.1021/acs.langmuir.0c00323
24. Li, H.; Hu, D.; Liang, F.; Huang, X.; Zhu, Q. Influence Factors on the Critical Micelle Concentration Determination Using Pyrene as a Probe and a Simple Method of Preparing Samples. *R. Soc. Open Sci.* **2020**, *7*, 192092. https://doi.org/10.1098/rsos.192092
25. Lu, Y.; Zhang, E.; Yang, J.; Cao, Z. Strategies to Improve Micelle Stability for Drug Delivery. *Nano Res.* **2018**, *11*, 4985–4998. https://doi.org/10.1007/s12274-018-2152-3
26. Perumal, S.; Atchudan, R.; Lee, W. A Review of Polymeric Micelles and Their Applications. *Polymers* **2022**, *14*, 2510. https://doi.org/10.3390/polym14122510
27. Roka, N.; Pitsikalis, M. Synthesis and Micellization Behavior of Amphiphilic Block Copolymers of Poly(N-Vinyl Pyrrolidone) and Poly(Benzyl Methacrylate): Block versus Statistical Copolymers. *Polymers* **2023**, *15*, 2225. https://doi.org/10.3390/polym15092225
28. Roka, N.; Pitsikalis, M. Synthesis, Characterization, and Self-Assembly Behavior of Block Copolymers of N-Vinyl Pyrrolidone with n-Alkyl Methacrylates. *Polymers* **2025**, *17*, 1122. https://doi.org/10.3390/polym17081122
29. Fokaidis-Psyllas, A.; Kokkorogianni, O.; Pitsikalis, M. Statistical Copolymers of N-Vinylpyrrolidone and Phenoxyethyl Methacrylate via RAFT Polymerization: Monomer Reactivity Ratios, Thermal Properties, Kinetics of Thermal Decomposition and Self-Assembly Behavior in Selective Solvents. *Polym. Bull.* **2025**. https://doi.org/10.1007/s00289-025-05885-2
30. Roka, N.; Skiadas, V.-C.; Kolovou, A.; Papazoglou, T.-P.; Pitsikalis, M. Micellization Studies of Block Copolymers of Poly(N-Vinyl Pyrrolidone) and Poly(Vinyl Esters) Bearing N-Alkyl Side-Groups in Tetrahydrofuran. *Polymers* to be submitted.
31. Kontoes-Georgoudakis, P.; Plachouras, N.V.; Kokkorogianni, O.; Pitsikalis, M. Amphiphilic Block Copolymers of Poly(N-Vinyl Pyrrolidone) and Poly(Isobornyl Methacrylate): Synthesis, Characterization and Micellization Behaviour in Selective Solvents. *Eur. Polym. J.* **2024**, *208*, 112873. https://doi.org/10.1016/j.eurpolymj.2024.112873
32. Roka, N.; Papazoglou, T.-P.; Pitsikalis, M. Block Copolymers of Poly(N-Vinyl Pyrrolidone) and Poly(Vinyl Esters) Bearing n-alkyl Side Groups via Reversible Addition-Fragmentation Chain-Transfer Polymerization: Synthesis, Characterization, and Thermal Properties. *Polymers* **2024**, *16*, 2447. https://doi.org/10.3390/polym16172447
33. Provencher, S.W. CONTIN: A general purpose constrained regularization program for inverting noisy linear algebraic and integral equations. *Comput. Phys. Commun.* **1982**, *27*, 229–242. https://doi.org/10.1016/0010-4655(82)90174-6

 doi:10.20944/preprints202509.2475.v1

34. Calzaferri, G.; Gfeller, N. Thionine in the Cage of Zeolite L. *J. Phys. Chem.* **1992**, *96* (8), 3428–3435. https://doi.org/10.1021/j100187a047
35. Roulia, M.; Vassiliadis, A.A. Clay-Catalyzed Phenomena of Cationic-Dye Aggregation and Hydroxo-Chromium Oligomerization. *Microporous Mesoporous Mater.* **2009**, *122* (1–3), 13–19. https://doi.org/10.1016/j.micromeso.2009.01.004
36. Jelley, E.E. Spectral Absorption and Fluorescence of Dyes in the Molecular State. *Nature* **1936**, *138* (3502), 1009–1010. https://doi.org/10.1038/1381009a0
37. Kobayashi, T. Excitons in J-Aggregates with Hierarchical Structure. *Supramol. Sci.* **1998**, *5* (3–4), 343–347. https://doi.org/10.1016/S0968-5677(98)00029-7